Hindawi
Andrologia
Volume 2023, Article ID 9222954, 9 pages
https://doi.org/10.1155/2023/9222954

Research Article

Compound Heterozygous Mutations in *FSIP2* Cause Morphological Abnormalities in Sperm Flagella Leading to Male Infertility

Fang Gao,[1,2] **Fei Ye**,[3] **Qian Zhang**,[3] **Yaoqiang Du**,[4] **Weihai Xu**,[2] **Ming Qi**,[2] **Guolian Ding**,[5] **Ling Zhang**,[2] **Chongyi Shu**,[2] **Xiaoyan Guo**,[2] **Shishi Li**,[2] **Min Zheng**,[2] **Liannv Qiu**,[6] **Amanda Zhou**,[7] **Liya Sun**,[7] **and Jing Shu**[2]

[1]*Zhejiang Chinese Medical University, Hangzhou, 310053 Zhejiang, China*
[2]*Center for Reproductive Medicine, Department of Reproductive Endocrinology, Zhejiang Provincial People's Hospital, Affiliated People's Hospital, Hangzhou Medical College, Hangzhou, 310014 Zhejiang, China*
[3]*College of Life Sciences and Medicine, Zhejiang Sci-Tech University, Hangzhou, 310023 Zhejiang, China*
[4]*Laboratory Medicine Center, Department of Transfusion Medicine, Zhejiang Provincial People's Hospital, Affiliated People's Hospital, Hangzhou Medical College, Hangzhou, 310014 Zhejiang, China*
[5]*Shanghai Key Laboratory of Embryo Original Disease, Shanghai, China and Obstetrics and Gynecology Hospital, Institute of Reproduction and Development, Fudan University, Shanghai 200011, China*
[6]*Laboratory Medicine Center, Department of Clinical Laboratory, Zhejiang Provincial People's Hospital Affiliated People's Hospital, Hangzhou Medical College, Hangzhou, Zhejiang 310014, China*
[7]*Kaiumph Medical Diagnostics Co., Ltd., Beijing 100050, China*

Correspondence should be addressed to Jing Shu; shujing@hmc.edu.cn

Received 10 October 2022; Revised 18 January 2023; Accepted 20 January 2023; Published 7 February 2023

Academic Editor: Marta Olszewska

Multiple morphological abnormalities of sperm flagella (MMAF) indicate severe teratozoospermia. The fibrous sheath interacting protein 2 (FSIP2) plays an important role in the normal construction of the flagella. In this study, a novel compound heterozygous mutation site of *FSIP2*, involving c.272_275delinsAGGTTTTTATA (p.L92Vfster74) and c.16788_16791del (p.E5596fs), was identified using whole-exome sequencing in a 32-year-old male. Electron microscope images revealed thick sperm neck, scattered sperm mitochondria, and short sperm tail. In addition, FSIP2 could not be visualized in sperm cells via immunofluorescence staining. Moreover, we used a protein domain prediction tool to identify a potential FSIP2 functional domain (5901-6774), the corresponding deletion of which was responsible for the MMAF phenotype in the infertile man. Finally, we reviewed the literature on *FSIP2* and found that *FSIP2* mutations are relatively concentrated, with high-frequency mutation regions in exon 16 and exon 17 accounting for 50% (10/20) and 35% (7/20) of cases, respectively. In conclusion, *FISP2* is a common pathogenic gene of MMAF, which may provide a rationale for genetic counseling in the next generation of patients with male infertility.

1. Introduction

The World Health Organization (WHO) reported that the incidence of infertility is approximately 8%–15% worldwide, and male factor accounts for approximately 50% of infertility cases, in which genetic factors are often involved [1, 2].

Whole-exome sequencing (WES) refers to high-throughput sequencing after the enrichment of the exon DNA sequence. It is an efficient technique for exploring genetic polymorphisms and mutations [3]. Several genes, including *AKAP3* (MIM604689) and *AKAP4* (MIM300185), are related to sperm structure and function, particularly the

normal composition of the sperm fibrous sheath. In addition, mutations in several genes, such as *DNAH1* (MIM603332), *CFAP43* (MIM617558), or *CFAP44* (MIM617559), can cause severe asthenozoospermia due to multiple morphological abnormalities of the sperm flagella (MMAF) [4–6].

Most pathological mutations in these genes can lead to severe axoneme structural disorganized and the loss of the sperm center doublet. Multiple morphological abnormalities of flagella (MMAF) is a sperm flagellar malformation, and the flagellar morphology is mostly presented as absent, coiled, bent, angulated, irregular, and short, which are some of the most severe sperm flagellar defects that leads to male infertility [7, 8]. Patients with mutations in these genes do not develop symptoms of primary ciliary dyskinesia (PCD), such as recurrent respiratory infections, bronchiectasis, and asthma [9, 10]. However, because MMAF is genetically heterogeneous, the known genetic defects only explain approximately 50%–60% of human MMAF cases. Thus, the relationship between genes and MMAF should be further explored [11, 12].

FSIP2 is the only gene that is focally amplified in 10% of testicular germ cell tumors, which are abnormalities with a strong biological basis [13, 14]. *FSIP2* was first reported in a male patient in 2018 [15]. *FSIP2* (OMIM 618153) is located on chromosome 2q32.1 and encodes a 6907-amino acid protein. Furthermore, FSIP2 attaches to the sperm tail by binding to AKAP4 and participates in fiber sheath assembly, and *FSIP2* mutation potentially leads to MMAF-associated asthenoteratospermia and male infertility [16].

We used WES in a sterile male patient with a high MMAF tendency toward sperm morphology. We identified novel compound heterozygous *FSIP2* variants with mutations c.272_275delinsAGGTTTTTATA (p.L92Vfster74) and c.16788_16791del (p.E5596fs). The present study provides useful evidence for the pathogenicity of these two mutations via electron microscopy and protein structure analysis. Thus, this study expands the significance of *FSIP2* genotyping in Chinese male patients with infertility.

2. Materials and Methods

2.1. Patient. The patient was a 32-year-old man who presented to the outpatient clinic of our hospital for semen examination due to fertility issues. Physical examination of the testis, epididymis, and vas deferens revealed normal findings; moreover, his blood hormone levels were within the normal range: follicle-stimulating hormone, 4.39 IU/L; luteinizing hormone, 1.5 IU/L; testosterone, 1.57 ng/mL; estradiol, 13.78 pg/mL; and prolactin, 17.7 ng/mL. Neither the patient nor his family had any PCD-related symptoms. The patient was diagnosed with asthenozoospermia and teratozoospermia based on three semen analyses. The control sample was obtained from a fertile man who was planning to have a second child. This study was approved by the Ethics Committee of Zhejiang Provincial People's Hospital, China (No. 2022091), and written informed consent was obtained from the patient (see Supplemental Material (available here)).

2.2. Semen Parameters and Sperm Morphological Analyses. The patient and healthy control were asked to abstain from sex for 2–7 days before collecting their masturbation semen samples in the hospital semen retrieval room. The semen samples were completely liquefied after being placed in a 37°C incubator for 30 min. Semen parameters, including semen volume, sperm progressive motility, and sperm concentration, were evaluated using computer-assisted sperm analysis (SAS medical, SAS-II, Beijing, China). Simultaneously, sperm morphology was assessed using Papanicolaou stain, and the samples were observed under bright field at 1,000x magnification. All semen parameters were evaluated according to the 5th edition of the WHO laboratory manual for the examination and processing of human semen [17].

2.3. Scanning Electron Microscopy (SEM). Prepared spermatozoa samples were immobilized overnight with 2.5% phosphate-buffered glutaraldehyde at 4°C. Immobilized spermatozoa samples were dehydrated using a series of 50%, 70%, and 90% graded ethanol, wherein the concentration was changed after every 15 min. Finally, the samples were incubated in 100% ethanol twice for 20 min each. After drying, the sperm samples were observed via SEM at 10 kV (Nova nano450, Thermo Fisher FEI).

2.4. Transmission Electron Microscopy (TEM). The prepared sperm samples were fixed overnight with 2.5% phosphate-buffered glutaraldehyde. These samples were washed thrice with 0.1 M phosphate buffer (PB; pH 7.2) and fixed with 1% osmium tetroxide in 0.1 M PB for 1 h at 4°C. Dehydration was performed sequentially using 50%, 70%, and 90% ethanol as well as 100% acetone. The samples were then allowed to polymerize for 48 h at 60°C. Subsequently, ultrathin sections were stained with 3% uranyl acetate and lead citrate. The ultrastructure of these samples was observed and photographed via TEM at 100 kV (Tecnai, Thermo Fisher FEI).

2.5. Immunostaining. The sperm samples were fixed on slides with 4% paraformaldehyde for 30 min. These samples were then permeabilized with 0.2% Triton-X for 15 min and blocked with 1% BSA for 60 min, followed by overnight incubation at 4°C with FSIP2 (rabbit monoclonal, Invitrogen, 1 : 100) and acetylated α-tubulin (mouse monoclonal, Santa Cruz, 1 : 200) antibodies. Next, the primary antibody was washed with PBS, and anti-rabbit (Abcam6802, 1 : 500, green) and anti-mouse (Abcam6789, 1 : 500, red) secondary antibodies were added to the slides and incubated with sperm for 1 h. Finally, the sperm samples were stained with DAPI for 3–5 min and observed under a scanning confocal immunofluorescence microscope (Leica sp8, Germany). Among the FSIP2 key domains, the protein domains were predicted using CDD (https://www.ncbi.nlm.nih.gov/Structure/cdd/wrpsb.cgi). Moreover, we visualized the 3D structural model of FSIP2 key domains using I-TASSER (http://zhang.bioinformatics.ku.edu/I-TASSER/) (see Supplemental Material) and PyMOL2.5.2 (https://pymol.org) to

Table 1: Results of the patient's three routine semen and strict sperm morphology.

	First ejaculate	Second ejaculate	Third ejaculate	Reference values[a]
Semen parameters				
Semen volume (mL)	4	3.5	4.0	≥1.5
Sperm concentration (10^6/mL)	111.7	107.6	111.3	≥15
Sperm progressive motility (%)	6.8	9.8	5.0	≥32
Sperm morphology				
Normal spermatozoa (%)	1	1	1	≥4
Anomalies of the head (%)	93	93	93	—
Short flagella (%)	71	68	75	—
Absent flagella (%)	0	1	1	—
Coiled flagella (%)	7	8	8	—
Flagella of irregular caliber (%)	2	4	2	—

[a]According to the World Health Organization standards (5th edition).

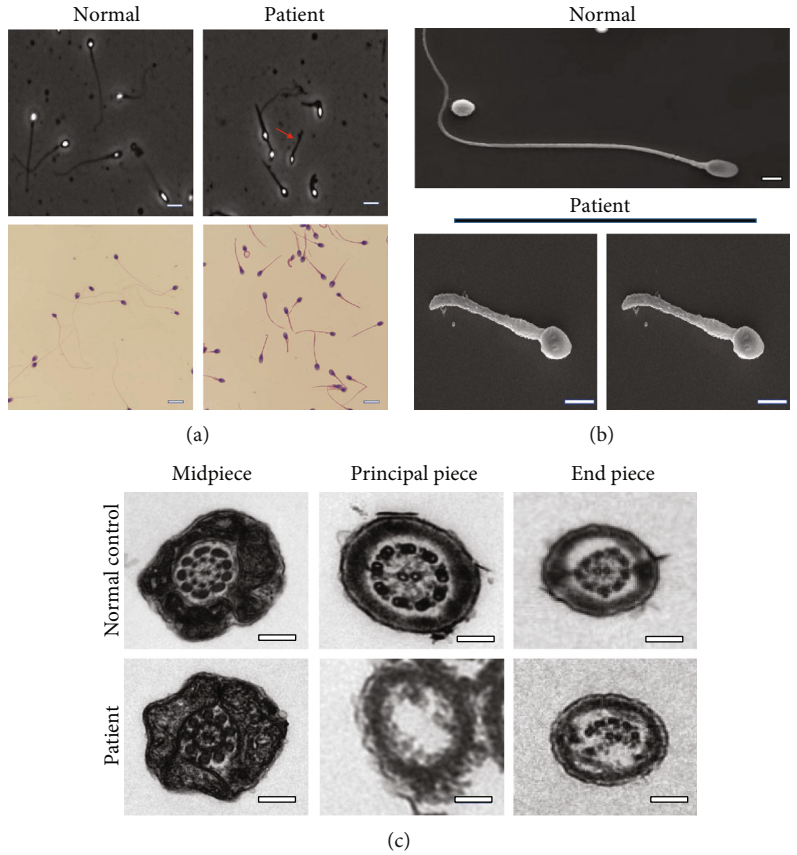

Figure 1: Comparison of morphology and ultrastructure of the control and patient sperm. (a) Papanicolaou-stained images of the control and patient sperm under light and oil microscopes. The patient's sperm is dominated by short tails (red arrows; scale bar: 10 μm). (b) Scanning electron microscope images of the control and patient sperm (scale bar: 10 μm). (c) Cross-sectional ultrastructure of the sperm in the control and patient under transmission electron microscope. In the patient, the central microtubules of the principal piece of the spermatozoa are missing, and the microtubule doublets are missing and disordered in the end piece (scale bar: 100 nm).

identify the impact of FSIP2 mutation sites on protein structure and function.

2.6. WES and Sanger Sequencing. Peripheral blood samples (2 mL) were collected from the patient and his parents, and DNA was extracted from whole blood using a blood genomic DNA extraction kit (QIAamp DNA Blood Mini Kit, Qiagen). WES was performed using Novaseq 6000 system based on Illumina sequencing technology. Patient gene sequences were aligned with normal human genome

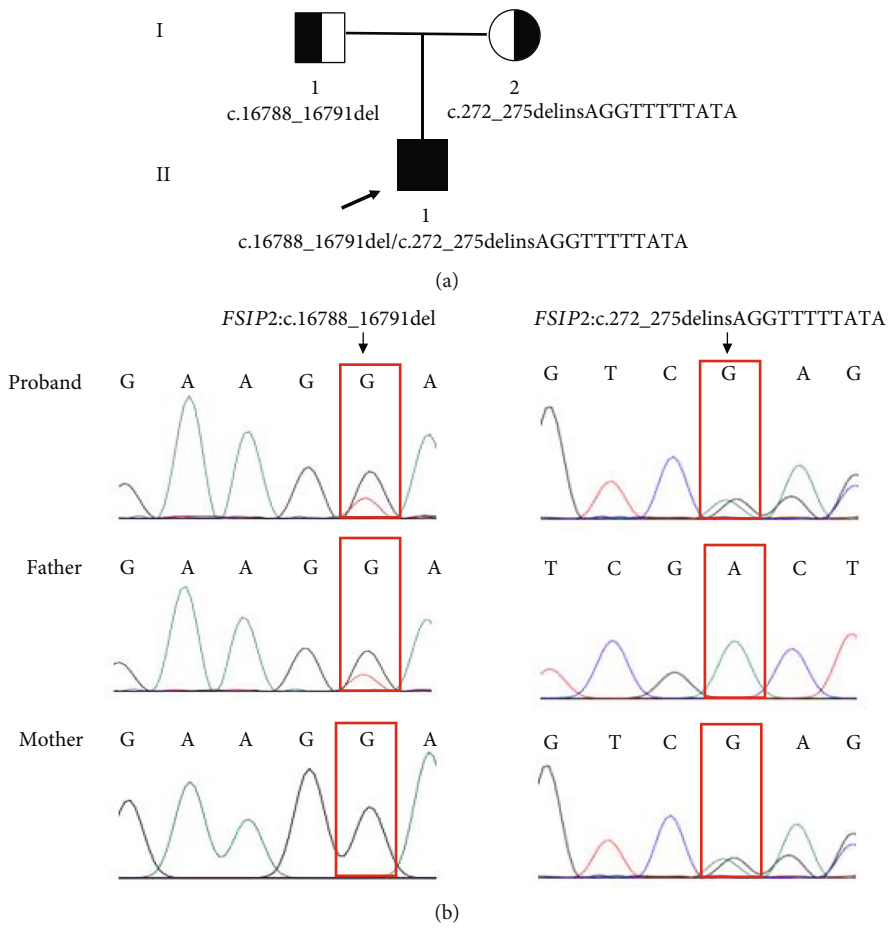

Figure 2: Recognition of compound heterozygous *FSIP2* mutation sites in the patient. (a) Family pedigree of the patient with *FSIP2* mutation. (b) Comparison of Sanger mutation locations in the patient and his parents. Mutation sites are marked using red boxes.

sequences, and loci with pathogenic potential were screened via Mutation Taster, SIFT, Polyphen2, and GERP++ software analysis and then matched according to genotype-phenotype. The frequency of genomic variants in the general population was assessed using 1,000 Genomes Project, ESP6500 and ExAC, and gnomADMAX (see Supplemental Material). FSIP2 mutations in the proband and patient's parents were verified using PCR and Sanger methods. The PCR cycle consists of three steps: (1) high-temperature denaturation, in which the DNA is converted to single strands at 95°; (2) low-temperature annealing (approximately 55°C), wherein the primer and single chain bind according to base complementary pairing; and (3) mid-temperature extension, in which the temperature is adjusted to the optimal reaction temperature of the DNA polymerase (approximately 72°C) to facilitate the synthesis of the complementary strand in the direction of the phosphate to five-carbon sugar (5′–3′). The following two primers were used to amplify exon 3 and exon 17 of *FSIP2* (5′→3′). Exon 3 (c.272_275delinsAGGTTTTTATA), forward: GGTGAGGAGAGAGGAAAGGA and reverse: ACCCACTTTATTATTGCTGGTGA. Exon 17 (16788_16791del), forward: TGAAAAGCGGCATGATTAACCT and reverse: TGGACTTCAAGGAGGATAACTGA. PCR products were sequenced using Ex Taq DNA Polymerase Kit (Bio-Rad, Hercules, CA, USA). Finally, sequence analysis was performed using 3730XL system (GSL Biotech).

3. Results

3.1. Routine Semen Analysis. Routine semen analysis revealed a normal sperm concentration and reduced sperm motility according to WHO guidelines (Table 1). Further, light microscopy and SEM analyses confirmed that approximately 90% of the patient's sperm had an abnormal morphology, including several short tails and a few curled flagella (Figures 1(a) and 1(b)). In both healthy control and patient, TEM analysis revealed that the cross-sectional ultrastructure of the sperm mid-piece exhibited an intact "9+2" axonal architecture. However, a cross-section of the principal piece and end piece of the patient's sperm revealed the loss of axonal structure and central pair (CP), with a disordered arrangement of the microtubule doublets (Figure 1(c)).

3.2. Gene Mutation Sites. Two novel *FSIP2* mutations, exon3: c.272_275delinsAGGTTTTTATA (p.L92Vfster74) and exon 17: c.16788_16791del (p.E5596fs), were identified

Table 2: In silico analysis of *FSIP2* mutations.

Gene*	Chromosome location #	Mutation	Amino acid change	Mutation type	Exon	SIFT	Polyphen2	Mutation taster	ExACMAX[a]	1000G_ALL[b]	GnomAD[c]	ACMG[d]
FSIP2	Chr2:186607906-186607909	c.272_275 delinsAGGTTTTTATA	p.L92Vfster74	Frameshift deletion/insertion	Exon 3	NA	NA	Disease-causing	0	0	0	Pathogenic
	Chr2:186670820-186670824	c.16788_16791del	p.S5597Gfster6	Frameshift deletion	Exon 17	NA	NA	Disease-causing	0	0	0	Pathogenic

Note: *Gene: *FSIP2* (NC_000002.12); #chromosome location: GRCh37/hg19 position; [a]ExAC: http://exac.broadinstitute.org; [b]1000G_ALL: ftp://ftp.1000genomes.ebi.ac.uk/vol1/ftp;[c]GnomAD: http://gnomad.broadinstitute.org; [d]ACMG: American College of Medical Genetics and Genomics.

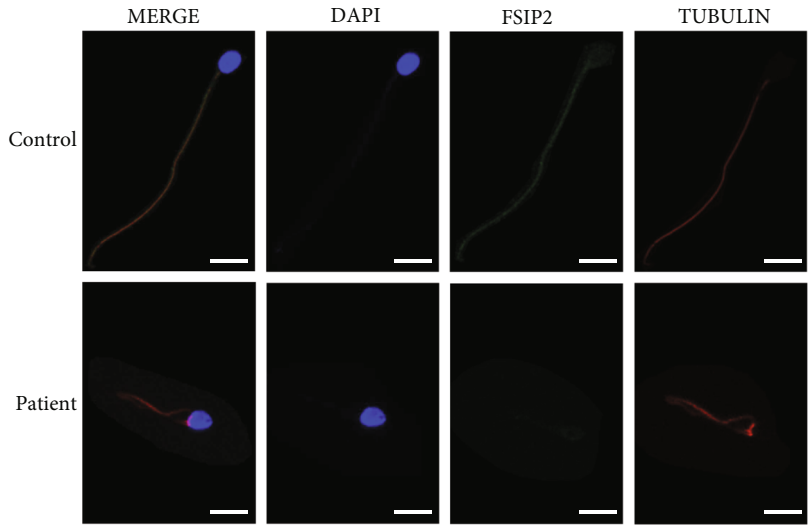

Figure 3: FSIP2 immunofluorescence staining in control and patient spermatozoa. FSIP2 immunofluorescence in control spermatozoa is shown in green; sperm flagella from a patient with an *FSIP2* mutation lack specific staining; acetylated tubulin is shown in red; sperm nuclear DNA stained with DAPI shown in blue (scale bar: 10 μm).

in the patient using WES (Figure 2). Detailed information on the variants is provided in Table 2. Sanger sequencing revealed that the patient's father had c.16788_16791del heterozygous mutation and his mother had c.272_275delinsAGGTTTTTATA heterozygous mutation (Figure 2(a)). Functional predictions based on SIFT and Polyphen2 databases suggested that these mutations have never been reported, whereas Mutation Taster classified them as disease-causing (Table 2). Both mutations (p.L92Vfster74 and p.E5596fs) are new mutations whose gene frequencies have not been described in ExACMAX, 1000G_ALL, or GnomAD (Table 2). The two mutation sites are pathogenic according to American College of Medical Genetics and Genomics (ACMG) guidelines (Table 2).

3.3. Analysis of the Sequence and Protein Structure of the FSIP2 Mutation Sites. FSIP2 expression in the patient and control samples was determined via immunofluorescence staining. The patient's sperm showed weak FSIP2 expression, whereas the control sperm showed positive FSIP2 expression (Figure 3).

To identify the mechanism underlying the loss of FSIP2 expression, we analyzed the sequence and protein structural features of the FSIP2 mutation site. We also compared the sequences of wild-type FSIP2 and the two patient mutation sites, c.272_275delinsAGGTTTTTATA and c.16788_16791del (Figure 4(a)). We found that c.272_275delinsAGGTTTTTATA mutation site ends early, leaving only 165 amino acids at the N-terminus, resulting in protein truncation. Notably, this serious deletion results in a significant loss of protein function. Furthermore, c.16788_16791del mutation site shared its first 5596 amino acids with wild-type FSIP2. However, subsequently, only five amino acids remained at the mutant C-terminus, whereas the wild-type C-terminus had a sequence of approximately 1400 amino acids.

Notably, the loss of informational sequence in c.272_275delinsAGGTTTTTATA resulted in the loss of protein structure and function. In the case of c.16788_16791del mutation, the loss of protein function can lead to the deletion of a key functional domain. To the best of our knowledge, the crystallographic structure of FSIP2 has not yet been reported in the literature. However, using a protein domain prediction tool, we could identify a potential functional domain in FSIP2 (5901-6774). In addition, we compared the sequences of FSIP1 and FSIP2 and found a sequence similarity of 12.5, indicating some structural similarity (see Supplemental Material). A structural model of FSIP2 and FSIP1 domains was constructed using homology modeling, which revealed the possible structure of the FSIP2 domain (5901-6774) (Figure 4(b)). The c.16788_16791del mutation led to the deletion of this critical domain, resulting in the loss of protein function and pathogenicity, as evidenced by the MMAF phenotype observed in this infertile patient.

4. Discussion

In this study, we identified novel *FSIP2* compound heterozygous mutation sites associated with short-tailed sperms in a Chinese man; the two new mutations were c.272_275delinsAGGTTTTTATA (p.L92Vfster74) and c.16788_16791del (p.E5596fs).

The sperm is composed of three parts: head, middle part, and tail [22]. The cytoskeleton of normal mobile sperm flagellum follows a "9+2" axonemal configuration and is surrounded by a fibrous sheath, mainly composed of nine outer microtubule doublets, two CPs, and an outer dense fiber [23–25]. Abnormal structure of the sperm fiber sheath and a lack of CP may cause MMAF, resulting in abnormal sperm tail morphology, including short, curly, or absent tails. In this study, a patient with *FSIP2* mutation had a

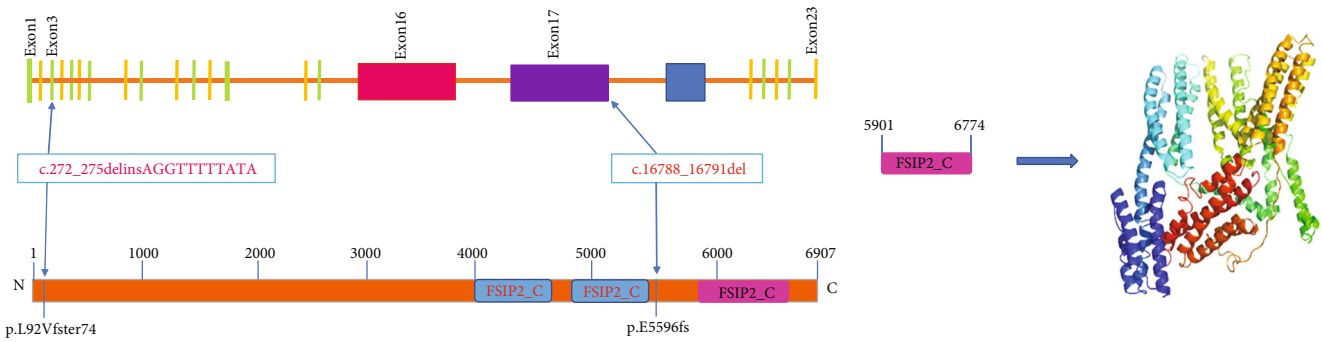

Figure 4: Variation in *FSIP2* exon positions and schematic diagram of the predicted FSIP2 domain. (a) The identified novel variants are shown in red, and the schematic diagram of the predicted FSIP2 domain is indicated in blue [15]. Domains affected by mutation sites in this study are shown in pink. (b) 3D cartoon model of the FSIP2 domain (5901-6774), indicated using rainbow.

Table 3: Summary of reported *FSIP2* gene mutation sites.

FSIP2 variants	Exon	Amino acid change	Status	Reference
c.910delC	Exon 8	p.Gln304Lys12ter3	ho	[15]
c.[1606_1607insTGT; 1607_1616delAAAGATTGCA]	Exon 16	p.Lys536Metfster1	ho	
c.2282dupA	Exon 16	p.Asn761llefster4	ho	
c.16389_16392delAATA	Exon 17	p.Glu5463Glufster7	ho	
c.1907C>A	Exon 16	p.S636ter	ho	[8]
c.8030_8031insA	Exon 16	p.T2680Nfster9	ho	
c.16246_16247insCCCAAATATCACC	Exon 16	p.T5416fster7	he	[18]
c.17323C>T	Exon 17	p.Q5774ter	he	
c.1750T>A	Exon 16	p.C584S	he	[19]
c.13600A>G	Exon 17	p.I4534V	he	
c.8368_8369insC	Exon 16	p.2790fs	ho	[20]
c.19981 C>T	Exon 18	p.R6661ter	he	[21]
c.18448G>A	Exon 17	p.V6150I	he	
c.5238-5240del	Exon 16	p.E1746del	he	
c.5480A>T	Exon 16	p.D1827V	he	
c.9056T>C	Exon 16	p.I3019T	he	
c.10823T>C	Exon 17	p.S5933F	he	
c.17798C>T	Exon 17	p.D1827V	he	
c.272_275delinsAGGTTTTTATA	Exon 3	p.L92Vfster74	he	This paper
c.16788_16791del	Exon 17	p.E5596fs	he	

Note: ho: homozygote; he: heterozygote.

normal sperm concentration, but the sperm showed loss of axonal structure and CPs, with disordered arrangement of the microtubule doublets. Moreover, in contrast to the sperm flagella of patients with *DNAH1*, *CFAP43*, and *CFAP44* mutations, those of patients with MMAF mostly contained short tails [26–28].

A major component of the skeletal structure of the sperm flagella is the fibrous sheath, and fibrous sheath dysplasia leads to male infertility [29]. Notably, *FSIP2* is unique to spermatogenic cells and may attach to sperm tails by binding to the fibrous sheath via AKAP4, although AKAP4 was not identified in any sperm samples from patients with *FSIP2* mutation [15]. Previous mouse model data suggest that *FSIP2* is only expressed in the testis [18, 30], and the FSIP2 protein emerges in the testis of mice 21 days after birth and gradually accumulates until adulthood. Moreover, *FSIP2* transcription begins in late spermatocyte developmental stage, and the gene is expressed in sperm cells and flagella at different spermatogenesis stages [18, 20]. Further, immunofluorescence staining was performed using the sperm samples of patients with *FSIP2* mutation and controls, which revealed that the FSIP2 antibody could not be observed in the piece of the sperm tail. However, after staining with tubulin, the fluorescence of both antibodies in the control group could be visualized. This suggests that *FSIP2* plays a major role in sperm tail formation. A recent study

reported that *FSIP2* mutations severely affect sperm acrosome development, suggesting that *FSIP2* mutations are responsible for the development of globozoospermia [21].

By analyzing the sequence and protein structure of *FSIP2* mutation sites, we identified a potential functional domain (5901-6774) that was affected by the mutations identified in the patient. The mutation ultimately leads to changes in sperm protein expression and function [15, 20]. Simultaneously, by combining the previously reported mutation sites in *FISP2* and those identified in the present study, we revealed that most of the 15 identified *FISP2* mutation sites were in exons 16 (50% [10 of 20]) and 17 (35% [7 of 20]), suggesting that the high-frequency *FSIP2* mutation region exists within these two exons with relatively concentrated features (Table 3).

Most sperms in patients with MMAF were immobile due to the completely defective flagella, and ICSI-assisted technology was used to address fertility problems in these patients. In a patient with FSIP2 mutation reported in 2021, two blastocysts were transferred after ICSI, but the outcome was unsuccessful [18]. Fortunately, in the patient with this newly reported FSIP2 compound heterozygous mutation (c.1750T>A and c.13600A>G), the embryos cultured on day 3 of the transfer resulted in a successful clinical pregnancy [19]. ICSI enables couples with obstructive azoospermia, severe oligospermia, or asthenospermia to have children. However, there are concerns about the health of these children because of the risk of genetic transmission via ICSI to male offspring [31]. As only few cases of FSIP2 mutation have been reported, more cases are needed to clarify the ART outcome of patients with *FSIP2* mutation.

In conclusion, we discovered a novel compound heterozygous mutation site in *FSIP2* that can cause male reproductive infertility and summarized the high-frequency *FSIP2* mutation sites. This finding may help clinicians better understand *FSIP2* to have a clear diagnostic basis for assessing asthenozoospermia.

Data Availability

The datasets generated during and/or analyzed during the current study are available from the corresponding author on reasonable request.

Conflicts of Interest

The authors declare no competing interests.

Acknowledgments

We would like to thank the participants described in this report for their consent and support. We also thank Professor Zhang Feng of Fudan University for his guidance. This study is supported by the Zhejiang Medical and Health Science and Technology Project (2019RC109 and 2020RC104).

Supplementary Materials

(1) The results of *FSIP2* mutation site query in ExAC and gnomADMAX; (2) scoring results of *FSIP2* structural model with I-TASSER; (3) sequence comparison results of *FSIP2* and *FSIP1*; (4) ethics approval. *(Supplementary Materials)*

References

[1] G. A. Ramaraju, S. Teppala, K. Prathigudupu et al., "Association between obesity and sperm quality," *Andrologia*, vol. 50, no. 3, 2018.

[2] Q. X. Wang, X. Wang, M. Y. Yu et al., "Random sperm DNA fragmentation index is not associated with clinical outcomes in day-3 frozen embryo transfer," *Asian Journal of Andrology*, vol. 24, no. 1, pp. 109–115, 2022.

[3] S. Kolmykov, G. Vasiliev, L. Osadchuk, M. Kleschev, and A. Osadchuk, "Whole-exome sequencing analysis of human semen quality in Russian multiethnic population," *Frontiers in Genetics*, vol. 12, article 662846, 2021.

[4] B. Baccetti, G. Collodel, M. Estenoz, D. Manca, E. Moretti, and P. Piomboni, "Gene deletions in an infertile man with sperm fibrous sheath dysplasia," *Human Reproduction*, vol. 20, no. 10, pp. 2790–2794, 2005.

[5] M. Ben Khelifa, C. Coutton, R. Zouari et al., "Mutations in _DNAH1_ , which encodes an inner arm heavy chain dynein, lead to male infertility from multiple morphological abnormalities of the sperm flagella," *American Journal of Human Genetics*, vol. 94, no. 1, pp. 95–104, 2014.

[6] C. Coutton, A. S. Vargas, A. Amiri-Yekta et al., "Mutations in CFAP43 and CFAP44 cause male infertility and flagellum defects in _Trypanosoma_ and human," *Nature Communications*, vol. 9, no. 1, p. 686, 2018.

[7] S. Y. Jiao, Y. H. Yang, and S. R. Chen, "Molecular genetics of infertility: loss-of-function mutations in humans and corresponding knockout/mutated mice," *Human Reproduction Update*, vol. 27, no. 1, pp. 154–189, 2021.

[8] W. Liu, X. He, S. Yang et al., "Bi-allelic mutations in _TTC21A_ induce asthenoteratospermia in humans and mice," *The American Journal of Human Genetics*, vol. 104, no. 4, pp. 738–748, 2019.

[9] A. Amiri-Yekta, C. Coutton, Z.-E. Kherraf et al., "Whole-exome sequencing of familial cases of multiple morphological abnormalities of the sperm flagella (MMAF) reveals new-DNAH1mutations," *Human Reproduction*, vol. 31, no. 12, pp. 2872–2880, 2016.

[10] J. F. Nsota Mbango, C. Coutton, C. Arnoult, P. F. Ray, and A. Toure, "Genetic causes of male infertility: snapshot on morphological abnormalities of the sperm flagellum," *Basic and Clinical Andrology*, vol. 29, no. 1, p. 2, 2019.

[11] C. Coutton, G. Martinez, Z.-E. Kherraf et al., "Bi-allelic mutations in _ARMC2_ lead to severe astheno-teratozoospermia due to sperm flagellum malformations in humans and mice," *American Journal of Human Genetics*, vol. 104, no. 2, pp. 331–340, 2019.

[12] Y. Yang, C. Jiang, X. Zhang et al., "Loss-of-function mutation in DNAH8 induces asthenoteratospermia associated with multiple morphological abnormalities of the sperm flagella," *Clinical Genetics*, vol. 98, no. 4, pp. 396–401, 2020.

[13] K. Litchfield, B. Summersgill, S. Yost et al., "Whole-exome sequencing reveals the mutational spectrum of testicular germ

cell tumours," *Nature Communications*, vol. 6, no. 1, p. 5973, 2015.

[14] Y. Zhang, X. Zhu, X. Qiao et al., "FSIP2 can serve as a predictive biomarker for clear cell renal cell carcinoma prognosis," *International Journal of Medical Sciences*, vol. 17, no. 17, pp. 2819–2825, 2020.

[15] G. Martinez, Z.-E. Kherraf, R. Zouari et al., "Whole-exome sequencing identifies mutations in FSIP2 as a recurrent cause of multiple morphological abnormalities of the sperm flagella," *Human Reproduction*, vol. 33, no. 10, pp. 1973–1984, 2018.

[16] K. Miki, W. D. Willis, P. R. Brown, E. H. Goulding, K. D. Fulcher, and E. M. Eddy, "Targeted disruption of the _Akap4_ gene causes defects in sperm flagellum and motility," *Developmental Biology*, vol. 248, no. 2, pp. 331–342, 2002.

[17] World Health Organization, *WHO Laboratory Manual for the Examination and Processing of Human Semen*, World Health Organization, Geneva, 5th edition, 2010.

[18] M. Liu, Y. Sun, Y. Li, J. Sun, Y. Yang, and Y. Shen, "Novel mutations in _FSIP2_ lead to multiple morphological abnormalities of the sperm flagella and poor ICSI prognosis," *Gene*, vol. 781, article 145536, 2021.

[19] Y. Yuan, W. Q. Xu, Z. Y. Chen et al., "Successful outcomes of intracytoplasmic sperm injection–embryo transfer using ejaculated spermatozoa from two Chinese asthenoteratozoospermic brothers with a compound heterozygous FSIP2 mutation," *Andrologia*, vol. 54, 2022.

[20] X. Fang, Y. Gamallat, Z. Chen et al., "Hypomorphic and hypermorphic mouse models of Fsip2 indicate its dosage-dependent roles in sperm tail and acrosome formation," *Development*, vol. 148, no. 11, 2021.

[21] R. Zheng, Y. Wang, Y. Li et al., "FSIP2 plays a role in the acrosome development during spermiogenesis," *Journal of Medical Genetics*, p. jmedgenet-2021-108406, 2022.

[22] J. Auger, "Assessing human sperm morphology: top models, underdogs or biometrics?," *Asian Journal of Andrology*, vol. 12, no. 1, pp. 36–46, 2010.

[23] J. Beurois, G. Martinez, C. Cazin et al., "CFAP70 mutations lead to male infertility due to severe astheno-teratozoospermia. A case report," *Human Reproduction*, vol. 34, no. 10, pp. 2071–2079, 2019.

[24] C. Jiang, X. Zhang, H. Zhang et al., "Novel bi-allelic mutations in DNAH1 cause multiple morphological abnormalities of the sperm flagella resulting in male infertility," *Translational Andrology and Urology*, vol. 10, no. 4, pp. 1656–1664, 2021.

[25] W. Zhao, Z. Li, P. Ping, G. Wang, X. Yuan, and F. Sun, "Outer dense fibers stabilize the axoneme to maintain sperm motility," *Journal of Cellular and Molecular Medicine*, vol. 22, no. 3, pp. 1755–1768, 2018.

[26] I. Khan, B. Shah, S. Dil et al., "Novel biallelic loss-of-function mutations in CFAP43 cause multiple morphological abnormalities of the sperm flagellum in Pakistani families," *Asian Journal of Andrology*, vol. 23, no. 6, pp. 627–632, 2021.

[27] Y. W. Sha, X. Wang, X. Xu et al., "Novel mutations in CFAP44 and CFAP43 cause multiple morphological abnormalities of the sperm flagella (MMAF)," *Reproductive Sciences*, vol. 26, no. 1, pp. 26–34, 2019.

[28] B. J. Zhuang, S. Y. Xu, L. Dong et al., "Novel DNAH1 mutation loci Lead to multiple morphological abnormalities of the sperm flagella and literature review," *Health*, vol. 40, no. 4, pp. 551–560, 2022.

[29] F. Jumeau, J. Sigala, F. Dossou-Gbete et al., "A-kinase anchor protein 4 precursor (pro-AKAP4) in human spermatozoa," *Andrology*, vol. 6, no. 6, pp. 854–859, 2018.

[30] P. R. Brown, K. Miki, D. B. Harper, and E. M. Eddy, "A-kinase anchoring protein 4 binding proteins in the fibrous sheath of the sperm flagellum," *Biology of Reproduction*, vol. 68, no. 6, pp. 2241–2248, 2003.

[31] L. Visser and S. Repping, "Unravelling the genetics of spermatogenic failure," *Reproduction*, vol. 139, no. 2, pp. 303–307, 2010.